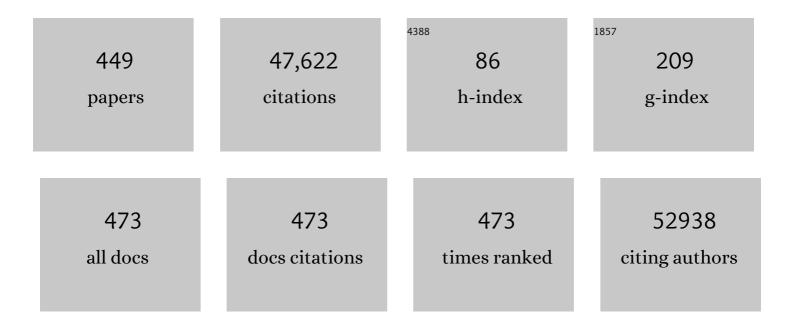
List of Publications by Year in descending order

Source: https://exaly.com/author-pdf/4007500/publications.pdf Version: 2024-02-01



FDIC STACH

#	Article	IF	CITATIONS
1	Shifts in valence states in bimetallic MXenes revealed by electron energy-loss spectroscopy (EELS). 2D Materials, 2022, 9, 025004.	4.4	11
2	Water-gas shift reaction over supported Au nanoparticles. Journal of Catalysis, 2022, 405, 475-488.	6.2	6
3	Dynamical Change of Valence States and Structure in NiCu <sub>3</sub> Nanoparticles during Redox Cycling. Journal of Physical Chemistry C, 2022, 126, 1991-2002.	3.1	14
4	Evidence for redispersion of Ni on LaMnO3 films following high-temperature oxidation. Journal of Catalysis, 2022, , .	6.2	10
5	Decoding reactive structures in dilute alloy catalysts. Nature Communications, 2022, 13, 832.	12.8	35
6	Light–matter coupling in large-area van der Waals superlattices. Nature Nanotechnology, 2022, 17, 182-189.	31.5	49
7	Higher loadings of Pt single atoms and clusters over reducible metal oxides: application to C–O bond activation. Catalysis Science and Technology, 2022, 12, 2920-2928.	4.1	7
8	Structural and spectroscopic characterization of pyrene derived carbon nano dots: a single-particle level analysis. Nanoscale, 2022, 14, 3568-3578.	5.6	6
9	Microwave Heating of Nanocrystals for Rapid, Low-Aggregation Intermetallic Phase Transformations. , 2022, 4, 823-830.		9
10	Dilute Alloys Based on Au, Ag, or Cu for Efficient Catalysis: From Synthesis to Active Sites. Chemical Reviews, 2022, 122, 8758-8808.	47.7	50
11	Synthesis and Characterization of Core-Shell Cu-Ru, Cu-Rh, and Cu-Ir Nanoparticles. Journal of the American Chemical Society, 2022, 144, 7919-7928.	13.7	13
12	High-Density, Localized Quantum Emitters in Strained 2D Semiconductors. ACS Nano, 2022, 16, 9651-9659.	14.6	21
13	Interfacial Reaction and Diffusion at the One-Dimensional Interface of Two-Dimensional PtSe <sub>2</sub> . Nano Letters, 2022, 22, 4733-4740.	9.1	3
14	Z-Contrast Enhancement in Au–Pt Nanocatalysts by Correlative X-ray Absorption Spectroscopy and Electron Microscopy: Implications for Composition Determination. ACS Applied Nano Materials, 2022, 5, 8775-8782.	5.0	3
15	Atomic Fe Dispersed Hierarchical Mesoporous Fe–N–C Nanostructures for an Efficient Oxygen Reduction Reaction. ACS Catalysis, 2021, 11, 74-81.	11.2	147
16	Anomalous metal vaporization from Pt/Pd/Al <sub>2</sub> O <sub>3</sub> under redox conditions. Nanoscale, 2021, 13, 11427-11438.	5.6	4
17	Mechanism and Kinetics of Methane Oxidation to Methanol Catalyzed by AuPd Nanocatalysts at Low Temperature. ACS Catalysis, 2021, 11, 2837-2845.	11.2	12
18	Direct Optoelectronic Imaging of 2D Semiconductor–3D Metal Buried Interfaces. ACS Nano, 2021, 15, 5618-5630.	14.6	35

#	Article	IF	CITATIONS
19	Subâ€Microsecond Polarization Switching in (Al,Sc)N Ferroelectric Capacitors Grown on Complementary Metal–Oxide–Semiconductorâ€Compatible Aluminum Electrodes. Physica Status Solidi - Rapid Research Letters, 2021, 15, 2000575.	2.4	39
20	Surface Facet Engineering in Nanoporous Gold for Low-Loading Catalysts in Aluminum–Air Batteries. ACS Applied Materials & Interfaces, 2021, 13, 13097-13105.	8.0	14
21	Resilient three-dimensional ordered architectures assembled from nanoparticles by DNA. Science Advances, 2021, 7, .	10.3	45
22	Insights into the Degradation Mechanism of Nanoporous Alloy-Type Li-Ion Battery Anodes. ACS Energy Letters, 2021, 6, 1749-1756.	17.4	29
23	Modified MAX Phase Synthesis for Environmentally Stable and Highly Conductive Ti <sub>3</sub> C <sub>2</sub> MXene. ACS Nano, 2021, 15, 6420-6429.	14.6	417
24	Post-CMOS Compatible Aluminum Scandium Nitride/2D Channel Ferroelectric Field-Effect-Transistor Memory. Nano Letters, 2021, 21, 3753-3761.	9.1	83
25	Efficacy of boron nitride encapsulation against plasma-processing of 2D semiconductor layers. Journal of Vacuum Science and Technology A: Vacuum, Surfaces and Films, 2021, 39, .	2.1	4
26	Nanoscale Chemical and Structural Analysis during <i>In Situ</i> Scanning/Transmission Electron Microscopy in Liquids. ACS Nano, 2021, 15, 10228-10240.	14.6	29
27	Aluminum scandium nitride-based metal–ferroelectric–metal diode memory devices with high on/off ratios. Applied Physics Letters, 2021, 118, .	3.3	49
28	Dilute Pd-in-Au alloy RCT-SiO2 catalysts for enhanced oxidative methanol coupling. Journal of Catalysis, 2021, 404, 943-953.	6.2	13
29	Quantifying Competitive Degradation Processes in Supported Nanocatalyst Systems. Nano Letters, 2021, 21, 5324-5329.	9.1	10
30	Nanoscale Structural and Chemical Properties of Ferroelectric Aluminum Scandium Nitride Thin Films. Journal of Physical Chemistry C, 2021, 125, 14394-14400.	3.1	11
31	In situ Transmission Electron Microscopy for Data-driven Modeling of Nanoparticle Evolution. Microscopy and Microanalysis, 2021, 27, 1312-1313.	0.4	1
32	Using In-Situ TEM to Investigate the Role of Lithium Iodide Addition to Lithium Thiophosphate. Microscopy and Microanalysis, 2021, 27, 3426-3427.	0.4	0
33	Electron energy loss spectroscopy of sub-10 nm 2D MoS2 crystals. Microscopy and Microanalysis, 2021, 27, 1210-1211.	0.4	0
34	Exploiting Microreactors for Correlative Studies of Working Catalysts With Electrons And X-Rays. Microscopy and Microanalysis, 2021, 27, 148-149.	0.4	0
35	Polyethylene Hydrogenolysis at Mild Conditions over Ruthenium on Tungstated Zirconia. Jacs Au, 2021, 1, 1422-1434.	7.9	95
36	Autonomous experimentation systems for materials development: A community perspective. Matter, 2021. 4. 2702-2726.	10.0	143

#	Article	IF	CITATIONS
37	Electrical breakdown strength enhancement in aluminum scandium nitride through a compositionally modulated periodic multilayer structure. Journal of Applied Physics, 2021, 130, .	2.5	11
38	Structural and Valence State Modification of Cobalt in CoPt Nanocatalysts in Redox Conditions. ACS Nano, 2021, 15, 20619-20632.	14.6	17
39	Achieving High Selectivity for Alkyne Hydrogenation at High Conversions with Compositionally Optimized PdAu Nanoparticle Catalysts in Raspberry Colloid-Templated SiO <sub>2</sub> . ACS Catalysis, 2020, 10, 441-450.	11.2	61
40	New Role of Pd Hydride as a Sensor of Surface Pd Distributions in Pdâ^'Au Catalysts. ChemCatChem, 2020, 12, 717-721.	3.7	12
41	Changes in Ni-NiO equilibrium due to LaFeO3 and the effect on dry reforming of CH4. Journal of Catalysis, 2020, 381, 561-569.	6.2	30
42	Using <i>in situ</i> and operando methods to characterize phase changes in charged lithium nickel cobalt aluminum oxide cathode materials. Journal Physics D: Applied Physics, 2020, 53, 113002.	2.8	12
43	Synthesis of Mo <sub>4</sub> VAlC <sub>4</sub> MAX Phase and Two-Dimensional Mo <sub>4</sub> VC <sub>4</sub> MXene with Five Atomic Layers of Transition Metals. ACS Nano, 2020, 14, 204-217.	14.6	429
44	In Situ Investigation of Chemomechanical Effects in Thiophosphate Solid Electrolytes. Matter, 2020, 3, 2138-2159.	10.0	67
45	Impact of Hierarchical Nanoporous Architectures on Sodium Storage in Antimony-Based Sodium-Ion Battery Anodes. ACS Applied Energy Materials, 2020, 3, 11231-11241.	5.1	11
46	Role of Lithium Iodide Addition to Lithium Thiophosphate: Implications beyond Conductivity. Chemistry of Materials, 2020, 32, 7150-7158.	6.7	12
47	Investigation of Rh–titanate (ATiO3) interactions on high-surface-area perovskite thin films prepared by atomic layer deposition. Journal of Materials Chemistry A, 2020, 8, 16973-16984.	10.3	12
48	Atomic-scale phase separation induced clustering of solute atoms. Nature Communications, 2020, 11, 3934.	12.8	11
49	Understanding important features of deep learning models for segmentation of high-resolution transmission electron microscopy images. Npj Computational Materials, 2020, 6, .	8.7	96
50	Tailoring Electronic and Optical Properties of MXenes through Forming Solid Solutions. Journal of the American Chemical Society, 2020, 142, 19110-19118.	13.7	198
51	Giant Gate-Tunability of Complex Refractive Index in Semiconducting Carbon Nanotubes. ACS Photonics, 2020, 7, 2896-2905.	6.6	16
52	Electron Transport in Dye-Sensitized TiO <sub>2</sub> Nanowire Arrays in Contact with Aqueous Electrolytes. Journal of Physical Chemistry C, 2020, 124, 22003-22010.	3.1	8
53	Zeolite Nanosheets Stabilize Catalyst Particles to Promote the Growth of Thermodynamically Unfavorable, Smallâ€Điameter Carbon Nanotubes. Small, 2020, 16, e2002120.	10.0	7
54	. Ferroelectric C-Axis Textured Aluminum Scandium Nitride Thin Films of 100 nm Thickness. , 2020, ,		18

#	Article	IF	CITATIONS
55	A Thermodynamic Investigation of Ni on Thin-Film Titanates (ATiO3). Inorganics, 2020, 8, 69.	2.7	7
56	Ferroelectric Switching in Sub-20 nm Aluminum Scandium Nitride Thin Films. IEEE Electron Device Letters, 2020, 41, 1774-1777.	3.9	55
57	Epitaxial and Strong Support Interactions between Pt and LaFeO <sub>3</sub> Films Stabilize Pt Dispersion. Journal of the American Chemical Society, 2020, 142, 10373-10382.	13.7	58
58	Maximization of carbon nanotube yield by solid carbon-assisted dewetting of iron catalyst films. Carbon, 2020, 165, 251-258.	10.3	10
59	Direct visualization of out-of-equilibrium structural transformations in atomically thin chalcogenides. Npj 2D Materials and Applications, 2020, 4, .	7.9	31
60	Stabilization of a nanoporous NiCu dilute alloy catalyst for non-oxidative ethanol dehydrogenation. Catalysis Science and Technology, 2020, 10, 5207-5217.	4.1	17
61	Changes in Ni-NiO Equilibrium Due to LaFeO3 and the Effect on Dry Reforming of CH4. Applied Catalysis B: Environmental, 2020, , 118798.	20.2	0
62	Low-Power Switching through Disorder and Carrier Localization in Bismuth-Doped Germanium Telluride Phase Change Memory Nanowires. ACS Nano, 2020, 14, 2162-2171.	14.6	13
63	Insights into the Promotion with Ru of Co/TiO <sub>2</sub> Fischer–Tropsch Catalysts: An In Situ Spectroscopic Study. ACS Catalysis, 2020, 10, 6042-6057.	11.2	39
64	Decomposition of Hydrogen Peroxide Catalyzed by AuPd Nanocatalysts during Methane Oxidation to Methanol. ACS Catalysis, 2020, 10, 5115-5123.	11.2	25
65	Enhancing catalytic performance of dilute metal alloy nanomaterials. Communications Chemistry, 2020, 3, .	4.5	41
66	Environmental TEM Studies Reveal Catalyst/Support Registry on 2D Zeolites. Microscopy and Microanalysis, 2019, 25, 1458-1459.	0.4	1
67	Using In-Situ Methods to Characterize Phase Changes in Charged Lithium Nickel Cobalt Aluminum Oxide Cathode Materials. Microscopy and Microanalysis, 2019, 25, 2030-2031.	0.4	2
68	Operando Electrochemical TEM of Solid-State Energy Storage Materials Using a Probe-Based Biasing Holder. Microscopy and Microanalysis, 2019, 25, 2108-2109.	0.4	0
69	Development of a Method to Characterize Active Sites in Photocatalysis using <i>operando</i> Transmission Electron Microscopy. Microscopy and Microanalysis, 2019, 25, 1444-1445.	0.4	1
70	Expanded lithiation of titanium disulfide: Reaction kinetics of multi-step conversion reaction. Nano Energy, 2019, 63, 103882.	16.0	21
71	Patterning Si at the 1 nm Length Scale with Aberrationâ€Corrected Electronâ€Beam Lithography: Tuning of Plasmonic Properties by Design. Advanced Functional Materials, 2019, 29, 1903429.	14.9	39
72	Tuning the Electrocatalytic Oxygen Reduction Reaction Activity of Pt–Co Nanocrystals by Cobalt Concentration with Atomic-Scale Understanding. ACS Applied Materials & Interfaces, 2019, 11, 26789-26797.	8.0	40

#	Article	IF	CITATIONS
73	"Intelligent―Pt Catalysts Studied on High-Surface-Area CaTiO <sub>3</sub> Films. ACS Catalysis, 2019, 9, 7318-7327.	11.2	39
74	Isolating the Roles of Hydrogen Exposure and Trace Carbon Contamination on the Formation of Active Catalyst Populations for Carbon Nanotube Growth. ACS Nano, 2019, 13, 8736-8748.	14.6	28
75	"Intelligent―Pt Catalysts Based on Thin LaCoO3 Films Prepared by Atomic Layer Deposition. Inorganics, 2019, 7, 113.	2.7	16
76	Characterization and Modeling of Coarsening Mechanisms in Supported Nanoparticle Ensemble Microscopy and Microanalysis, 2019, 25, 1420-1421.	0.4	0
77	Evolution of steady-state material properties during catalysis: Oxidative coupling of methanol over nanoporous Ag0.03Au0.97. Journal of Catalysis, 2019, 380, 366-374.	6.2	24
78	Optimized High-Temperature In-Situ Transmission Electron Microscopy Double-Tilt Sample Heating Platform. Microscopy and Microanalysis, 2019, 25, 1540-1541.	0.4	0
79	Carbon-assisted catalyst pretreatment enables straightforward synthesis of high-density carbon nanotube forests. Carbon, 2019, 153, 196-205.	10.3	31
80	Phase evolution of conversion-type electrode for lithium ion batteries. Nature Communications, 2019, 10, 2224.	12.8	99
81	Quantification of Charge Transfer at the Interfaces of Oxide Thin Films. Journal of Physical Chemistry A, 2019, 123, 4632-4637.	2.5	5
82	Impact of Synthesis Method on Phase Transformations of Layered Lithium Vanadium Oxide upon Electrochemical (De)lithiation. Journal of the Electrochemical Society, 2019, 166, A771-A778.	2.9	10
83	The Influence of Surface Platinum Deposits on the Photocatalytic Activity of Anatase TiO <sub>2</sub> Nanocrystals. Journal of Physical Chemistry C, 2019, 123, 10477-10486.	3.1	7
84	Cathodoluminescence as an effective probe of carrier transport and deep level defects in droop-mitigating InGaN/GaN quantum well heterostructures. Applied Physics Express, 2019, 12, 034003.	2.4	2
85	A Study of Support Effects for CH4 and CO Oxidation over Pd Catalysts on ALD-Modified Al2O3. Catalysis Letters, 2019, 149, 905-915.	2.6	30
86	1â€nm Si Patterning: Patterning Si at the 1 nm Length Scale with Aberration orrected Electronâ€Beam Lithography: Tuning of Plasmonic Properties by Design (Adv. Funct. Mater. 52/2019). Advanced Functional Materials, 2019, 29, 1970353.	14.9	2
87	Quantitative measurement of contact area and electron transport across platinum nanocontacts for scanning probe microscopy and electrical nanodevices. Nanotechnology, 2019, 30, 045705.	2.6	14
88	Size-dependent kinetics during non-equilibrium lithiation of nano-sized zinc ferrite. Nature Communications, 2019, 10, 93.	12.8	39
89	Order in one dimension. Nature Materials, 2019, 18, 4-6.	27.5	4
90	Surface Crystallization of Liquid Au–Si and Its Impact on Catalysis. Advanced Materials, 2019, 31, 1806544.	21.0	23

#	Article	IF	CITATIONS
91	Synthesis and Characterization of CuFe <sub>2</sub> O <sub>4</sub> Nano/Submicron Wire–Carbon Nanotube Composites as Binder-free Anodes for Li-Ion Batteries. ACS Applied Materials & Interfaces, 2018, 10, 8770-8785.	8.0	42
92	Synthesis, Structural Characterization, and Growth Mechanism of Li <sub>1+<i>x</i></sub> V <sub>3</sub> O <sub>8</sub> Submicron Fibers for Lithium-Ion Batteries. Crystal Growth and Design, 2018, 18, 2055-2066.	3.0	13
93	In situimaging of the soldering reactions in nanoscale Cu/Sn/Cu and Sn/Cu/Sn diffusion couples. Journal of Applied Physics, 2018, 123, 024302.	2.5	3
94	Growth of Nanoparticles with Desired Catalytic Functions by Controlled Doping-Segregation of Metal in Oxide. Chemistry of Materials, 2018, 30, 1585-1592.	6.7	11
95	Evolution and stabilization of subnanometric metal species in confined space by in situ TEM. Nature Communications, 2018, 9, 574.	12.8	140
96	Structural and Electrochemical Characteristics of Ca-Doped "Flower-like― Li <sub>4</sub> Ti <sub>5</sub> O <sub>12</sub> Motifs as High-Rate Anode Materials for Lithium-Ion Batteries. Chemistry of Materials, 2018, 30, 671-684.	6.7	76
97	Two-Dimensional Holey Nanoarchitectures Created by Confined Self-Assembly of Nanoparticles <i>via</i> Block Copolymers: From Synthesis to Energy Storage Property. ACS Nano, 2018, 12, 820-828.	14.6	62
98	Capacity Fading Mechanism of the Commercial 18650 LiFePO <sub>4</sub> -Based Lithium-Ion Batteries: An in Situ Time-Resolved High-Energy Synchrotron XRD Study. ACS Applied Materials & Interfaces, 2018, 10, 4622-4629.	8.0	40
99	Atomic-Scale Insights into the Oxidation of Aluminum. ACS Applied Materials & Interfaces, 2018, 10, 2230-2235.	8.0	95
100	Identifying Dynamic Structural Changes of Active Sites in Pt–Ni Bimetallic Catalysts Using Multimodal Approaches. ACS Catalysis, 2018, 8, 4120-4131.	11.2	54
101	Molecular structure and sour gas surface chemistry of supported K2O/WO3/Al2O3 catalysts. Applied Catalysis B: Environmental, 2018, 232, 146-154.	20.2	19
102	Dislocation nucleation facilitated by atomicÂsegregation. Nature Materials, 2018, 17, 56-63.	27.5	99
103	In-situ Atomic-Resolution Observations of Oxide-Reduction Induced Formation of Nano-Holes in Cu2O Thin Films. Microscopy and Microanalysis, 2018, 24, 1816-1817.	0.4	0
104	Probing enhanced lithium-ion transport kinetics in 2D holey nanoarchitectured electrodes. Nano Futures, 2018, 2, 035008.	2.2	15
105	Revisiting Conversion Reaction Mechanisms in Lithium Batteries: Lithiation-Driven Topotactic Transformation in FeF <sub>2</sub> . Journal of the American Chemical Society, 2018, 140, 17915-17922.	13.7	41
106	Carbon Nanotubes and Related Nanomaterials: Critical Advances and Challenges for Synthesis toward Mainstream Commercial Applications. ACS Nano, 2018, 12, 11756-11784.	14.6	388
107	Single-Digit Nanometer Electron-Beam Lithography with an Aberration-Corrected Scanning Transmission Electron Microscope. Journal of Visualized Experiments, 2018, , .	0.3	4
108	Segregation induced order-disorder transition in Cu(Au) surface alloys. Acta Materialia, 2018, 154, 220-227.	7.9	11

#	Article	IF	CITATIONS
109	Highly active subnanometer Rh clusters derived from Rh-doped SrTiO3 for CO2 reduction. Applied Catalysis B: Environmental, 2018, 237, 1003-1011.	20.2	67
110	Improved Coking Resistance of "Intelligent―Ni Catalysts Prepared by Atomic Layer Deposition. ACS Catalysis, 2018, 8, 7679-7687.	11.2	59
111	Towards Real Time Quantitative Analysis of Supported Nanoparticle Ensemble Evolution Investigated by Environmental TEM. Microscopy and Microanalysis, 2018, 24, 540-541.	0.4	2
112	Using Operando Characterization, Data Analytics, and Artificial Intelligence to Understand Mechanistic Links between Processing and Structure. Microscopy and Microanalysis, 2018, 24, 258-259.	0.4	0
113	Achieving High Cycling Rates via In Situ Generation of Active Nanocomposite Metal Anodes. ACS Applied Energy Materials, 2018, 1, 4651-4661.	5.1	19
114	Anatomy of a Visible Light Activated Photocatalyst for Water Splitting. ACS Catalysis, 2018, 8, 6650-6658.	11.2	24
115	<i>In situ</i> atomic-scale observation of inhomogeneous oxide reduction. Chemical Communications, 2018, 54, 7342-7345.	4.1	8
116	Atomic Insight into the Layered/Spinel Phase Transformation in Charged LiNi <sub>0.80</sub> Co <sub>0.15</sub> Al <sub>0.05</sub> O <sub>2</sub> Cathode Particles. Journal of Physical Chemistry C, 2017, 121, 1421-1430.	3.1	52
117	Plasmonic Titanium Nitride Nanostructures via Nitridation of Nanopatterned Titanium Dioxide. Advanced Optical Materials, 2017, 5, 1600717.	7.3	42
118	Length-dependent melting behavior of Sn nanowires. Journal of Materials Research, 2017, 32, 1194-1202.	2.6	9
119	Investigation of Structural Evolution of Li <sub>1.1</sub> V <sub>3</sub> O <sub>8</sub> by <i>In Situ</i> X-ray Diffraction and Density Functional Theory Calculations. Chemistry of Materials, 2017, 29, 2364-2373.	6.7	40
120	Importance of Low Dimensional CeOx Nanostructures in Pt/CeOx–TiO2 Catalysts for the Water–Gas Shift Reaction. Journal of Physical Chemistry C, 2017, 121, 6635-6642.	3.1	17
121	Correlating Preparative Approaches with Electrochemical Performance of Fe <sub>3</sub> O <sub>4</sub> -MWNT Composites Used as Anodes in Li-Ion Batteries. ECS Journal of Solid State Science and Technology, 2017, 6, M3122-M3131.	1.8	13
122	Plasmonics: Plasmonic Titanium Nitride Nanostructures via Nitridation of Nanopatterned Titanium Dioxide (Advanced Optical Materials 7/2017). Advanced Optical Materials, 2017, 5, .	7.3	0
123	Aberration-Corrected Electron Beam Lithography at the One Nanometer Length Scale. Nano Letters, 2017, 17, 4562-4567.	9.1	80
124	Strain Coupling of Conversionâ€ŧype Fe <sub>3</sub> O <sub>4</sub> Thin Films for Lithium Ion Batteries. Angewandte Chemie - International Edition, 2017, 56, 7813-7816.	13.8	59
125	Strain Coupling of Conversionâ€ŧype Fe 3 O 4 Thin Films for Lithium Ion Batteries. Angewandte Chemie, 2017, 129, 7921-7924.	2.0	2
126	Visualization of structural evolution and phase distribution of a lithium vanadium oxide (Li <sub>1.1</sub> V <sub>3</sub> O <sub>8</sub> ) electrode via an operando and in situ energy dispersive X-ray diffraction technique. Physical Chemistry Chemical Physics, 2017, 19, 14160-14169.	2.8	25

#	Article	IF	CITATIONS
127	Conductive Polymers: A Tunable 3D Nanostructured Conductive Gel Framework Electrode for Highâ€Performance Lithium Ion Batteries (Adv. Mater. 22/2017). Advanced Materials, 2017, 29, .	21.0	1
128	Lithium Vanadium Oxide (Li <sub>1.1</sub> V <sub>3</sub> O <sub>8</sub> ) Coated with Amorphous Lithium Phosphorous Oxynitride (LiPON): Role of Material Morphology and Interfacial Structure on Resulting Electrochemistry. Journal of the Electrochemical Society, 2017, 164, A1503-A1513.	2.9	9
129	Intergranular Cracking as a Major Cause of Long-Term Capacity Fading of Layered Cathodes. Nano Letters, 2017, 17, 3452-3457.	9.1	361
130	Energy Dispersive X-ray Diffraction (EDXRD) of Li1.1V3O8 Electrochemical Cell. MRS Advances, 2017, 2, 401-406.	0.9	8
131	A Tunable 3D Nanostructured Conductive Gel Framework Electrode for Highâ€Performance Lithium Ion Batteries. Advanced Materials, 2017, 29, 1603922.	21.0	175
132	Dynamic restructuring drives catalytic activity on nanoporous gold–silver alloy catalysts. Nature Materials, 2017, 16, 558-564.	27.5	243
133	Interface dynamics in one-dimensional nanoscale Cu/Sn couples. Acta Materialia, 2017, 125, 136-144.	7.9	24
134	Structural Change of a Cu/ZnO Catalyst under Methanol Observed by ETEM. Microscopy and Microanalysis, 2017, 23, 2100-2101.	0.4	2
135	In-Situ TEM Study of Phase Evolution in Individual Battery Materials. Microscopy and Microanalysis, 2017, 23, 2008-2009.	0.4	Ο
136	The Intermediate State of the Layered → Spinel Phase Transformation in LiNi <sub>0.80</sub> Co <sub>0.15</sub> Al <sub>0.05</sub> O <sub>2</sub> Cathode. Microscopy and Microanalysis, 2017, 23, 2014-2015.	0.4	1
137	In situ atomic-scale imaging of the metal/oxide interfacial transformation. Nature Communications, 2017, 8, 307.	12.8	79
138	Atomic level cleaning of poly-methyl-methacrylate residues from the graphene surface using radiolized water at high temperatures. Applied Physics Letters, 2017, 111, .	3.3	13
139	A Microporous and Naturally Nanostructured Thermoelectric Metal-Organic Framework with Ultralow Thermal Conductivity. Joule, 2017, 1, 168-177.	24.0	159
140	Signature of Metallic Behavior in the Metal–Organic Frameworks M <sub>3</sub> (hexaiminobenzene) <sub>2</sub> (M = Ni, Cu). Journal of the American Chemical Society, 2017, 139, 13608-13611.	13.7	324
141	Enhanced Carbon Dioxide Electroreduction to Carbon Monoxide over Defectâ€Rich Plasmaâ€Activated Silver Catalysts. Angewandte Chemie, 2017, 129, 11552-11556.	2.0	58
142	Enhanced Carbon Dioxide Electroreduction to Carbon Monoxide over Defectâ€Rich Plasmaâ€Activated Silver Catalysts. Angewandte Chemie - International Edition, 2017, 56, 11394-11398.	13.8	180
143	Multimodal Study of the Speciations and Activities of Supported Pd Catalysts During the Hydrogenation of Ethylene. Journal of Physical Chemistry C, 2017, 121, 18962-18972.	3.1	24
144	Atomically Visualizing Elemental Segregation-Induced Surface Alloying and Restructuring. Journal of Physical Chemistry Letters, 2017, 8, 6035-6040.	4.6	10

#	Article	IF	CITATIONS
145	Visualization of Phase Evolution of Ternary Spinel Transition Metal Oxides (CuFe <sub>2</sub> O <sub>4</sub> ) during Lithiation. Microscopy and Microanalysis, 2017, 23, 2022-2023.	0.4	1
146	Experimental Study of the Detection Limit in Dual-Gate Biosensors Using Ultrathin Silicon Transistors. ACS Nano, 2017, 11, 7142-7147.	14.6	28
147	Making Li-metal electrodes rechargeable by controlling the dendrite growth direction. Nature Energy, 2017, 2, .	39.5	355
148	Nanoscale structural oscillations in perovskite oxides induced by oxygen evolution. Nature Materials, 2017, 16, 121-126.	27.5	149
149	Operando and multimodal studies of speciation and activity of Pt catalysts during the hydrogenation of ethylene. Microscopy and Microanalysis, 2017, 23, 892-893.	0.4	0
150	The Stability of Sapphire in the Presence of Water: an Environmental TEM Study. Microscopy and Microanalysis, 2017, 23, 964-965.	0.4	1
151	Automated image acquisition and analysis of beam sensitive samples. Microscopy and Microanalysis, 2017, 23, 1788-1789.	0.4	0
152	Glucose sensing using dual-gated BioFETs with 5nm-thick silicon body. , 2017, , .		0
153	Near real time ETEM streaming video analysis. , 2017, , .		0
154	Investigating load-dependent conduction through platinum nanocontacts using in situ electromechanical testing inside a transmission electron microscope. , 2017, , .		1
155	Development of Real-Time Probe Current Calibration for Performing Quantitative STEM with a Cold Field-Emission Gun Microscopy and Microanalysis, 2016, 22, 940-941.	0.4	0
156	Direct Visualization of Lithium Intercalation in Spinel Iron Oxide by In-Situ Bright-Field Scanning Transmission Electron Microscopy. Microscopy and Microanalysis, 2016, 22, 760-761.	0.4	1
157	Combining post-specimen aberration correction and direct electron detection to image molecular structure in liquid crystal polymers. Microscopy and Microanalysis, 2016, 22, 1924-1925.	0.4	5
158	Polyvinylpyrrolidone-induced anisotropic growth of gold nanoprisms in plasmon-driven synthesis. Nature Materials, 2016, 15, 889-895.	27.5	239
159	Analysis of nanoparticle growth in environmental transmission electron microscopy. , 2016, , .		2
160	Determination of the mechanism and extent of surface degradation in Ni-based cathode materials after repeated electrochemical cycling. APL Materials, 2016, 4, .	5.1	24
161	Interrogation of bimetallic particle oxidation in three dimensions at the nanoscale. Nature Communications, 2016, 7, 13335.	12.8	65
162	Visualizing non-equilibrium lithiation of spinel oxide via in situ transmission electron microscopy. Nature Communications, 2016, 7, 11441.	12.8	162

#	Article	IF	CITATIONS
163	ETEM Study of Oxygen Activity in LiNi 0.8 Co 0.15 Al 0.05 O 2 (NCA) Cathode Materials at Various States of Charge. Microscopy and Microanalysis, 2016, 22, 1332-1333.	0.4	1
164	Understanding the Rocksalt-to-Wurtzite phase transformation through microstructural analysis of (Al,Sc)N epitaxial thin films. Applied Physics Letters, 2016, 109, .	3.3	15
165	Elucidating the Sole Contribution from Electromagnetic Nearâ€Fields in Plasmonâ€Enhanced Cu <sub>2</sub> O Photocathodes. Advanced Energy Materials, 2016, 6, 1501250.	19.5	31
166	Tuning the Activity of Oxygen in LiNi <sub>0.8</sub> Co <sub>0.15</sub> Al <sub>0.05</sub> O <sub>2</sub> Battery Electrodes. ACS Applied Materials & Interfaces, 2016, 8, 27762-27771.	8.0	58
167	Controlling the Formation and Structure of Nanoparticle Superlattices through Surface Ligand Behavior. Langmuir, 2016, 32, 11606-11614.	3.5	9
168	Current status and future directions for in situ transmission electron microscopy. Ultramicroscopy, 2016, 170, 86-95.	1.9	181
169	Real-Time Imaging of Self-Organization and Mechanical Competition in Carbon Nanotube Forest Growth. ACS Nano, 2016, 10, 11496-11504.	14.6	34
170	Kinetic Phase Evolution of Spinel Cobalt Oxide during Lithiation. ACS Nano, 2016, 10, 9577-9585.	14.6	54
171	Development of a New Generation of Stable, Tunable, and Catalytically Active Nanoparticles Produced by the Helium Nanodroplet Deposition Method. Journal of Physical Chemistry Letters, 2016, 7, 2910-2914.	4.6	21
172	Reversed Nanoscale Kirkendall Effect in Au–InAs Hybrid Nanoparticles. Chemistry of Materials, 2016, 28, 8032-8043.	6.7	25
173	Charge transport in CdTe solar cells revealed by conductive tomographic atomic force microscopy. Nature Energy, 2016, 1, .	39.5	66
174	High-pressure vapor-phase hydrodeoxygenation of lignin-derived oxygenates to hydrocarbons by a PtMo bimetallic catalyst: Product selectivity, reaction pathway, and structural characterization. Journal of Catalysis, 2016, 344, 535-552.	6.2	58
175	Correlating Titania Nanostructured Morphologies with Performance as Anode Materials for Lithium-Ion Batteries. ACS Sustainable Chemistry and Engineering, 2016, 4, 6299-6312.	6.7	29
176	Highly selective plasma-activated copper catalysts for carbon dioxide reduction to ethylene. Nature Communications, 2016, 7, 12123.	12.8	896
177	Measurement of the Dewetting, Nucleation, and Deactivation Kinetics of Carbon Nanotube Population Growth by Environmental Transmission Electron Microscopy. Chemistry of Materials, 2016, 28, 3804-3813.	6.7	41
178	High-Energy Surface and Volume Plasmons in Nanopatterned Sub-10 nm Aluminum Nanostructures. Nano Letters, 2016, 16, 4149-4157.	9.1	38
179	Redox chemistry of a binary transition metal oxide (AB <sub>2</sub> O <sub>4</sub> ): a study of the Cu <sup>2+</sup> /Cu <sup>0</sup> and Fe <sup>3+</sup> /Fe <sup>0</sup> interconversions observed upon lithiation in a CuFe <sub>2</sub> O <sub>4</sub> battery using X-ray absorption spectroscopy. Physical Chemistry Chemical Physics. 2016. 18. 16930-16940.	2.8	21
180	Statistical analysis of support thickness and particle size effects in HRTEM imaging of metal nanoparticles. Ultramicroscopy, 2016, 169, 22-29.	1.9	11

#	Article	IF	CITATIONS
181	Unraveling the Hydrogenation of TiO <sub>2</sub> and Graphene Oxide/TiO <sub>2</sub> Composites in Real Time by in Situ Synchrotron X-ray Powder Diffraction and Pair Distribution Function Analysis. Journal of Physical Chemistry C, 2016, 120, 3472-3482.	3.1	16
182	Metal–metal chalcogenide molecular precursors to binary, ternary, and quaternary metal chalcogenide thin films for electronic devices. Chemical Communications, 2016, 52, 5007-5010.	4.1	59
183	Nanowire growth kinetics in aberration corrected environmental transmission electron microscopy. Chemical Communications, 2016, 52, 5686-5689.	4.1	20
184	Atomic Resolution in Situ Imaging of a Double-Bilayer Multistep Growth Mode in Gallium Nitride Nanowires. Nano Letters, 2016, 16, 2283-2288.	9.1	34
185	The Effect of the Surface Composition of Ru-Pt Bimetallic Catalysts for Methanol Oxidation. Electrochimica Acta, 2016, 195, 106-111.	5.2	37
186	Direct observation of morphological evolution of a catalyst during carbon nanotube forest growth: new insights into growth and growth termination. Nanoscale, 2016, 8, 2055-2062.	5.6	14
187	Oxidation-state sensitive imaging of cerium dioxide by atomic-resolution low-angle annular dark field scanning transmission electron microscopy. Ultramicroscopy, 2016, 162, 52-60.	1.9	11
188	An in situ phosphorus source for the synthesis of Cu <sub>3</sub> P and the subsequent conversion to Cu <sub>3</sub> PS <sub>4</sub> nanoparticle clusters. Journal of Materials Research, 2015, 30, 3710-3716.	2.6	10
189	Characterizing Working Catalysts with Correlated Electron and Photon Probes. Microscopy and Microanalysis, 2015, 21, 563-564.	0.4	2
190	Development of Quantitative STEM for a Conventional S/TEM and Real-Time Current Calibration for Performing QSTEM with a Cold Field Emission Gun. Microscopy and Microanalysis, 2015, 21, 2127-2128.	0.4	1
191	In situ Studies of the Reaction-Driven Restructuring of Ni-Co Core-Shell Nanoparticles. Microscopy and Microanalysis, 2015, 21, 637-638.	0.4	4
192	Comparison of Co3O4 and CoO Nanoparticles as Anodes for Lithium-ion Batteries. Microscopy and Microanalysis, 2015, 21, 477-478.	0.4	2
193	Operando Characterization of Catalysts through use of a Portable Microreactor. ChemCatChem, 2015, 7, 3683-3691.	3.7	29
194	Contrasting Reaction Modality between Electrochemical Sodiation and Lithiation in NiO Conversion Electrode Materials. Microscopy and Microanalysis, 2015, 21, 325-326.	0.4	2
195	Revealing Near-Surface to Interior Redox upon Lithiation in Conversion Electrode Materials Using Electron Microscopy. Microscopy and Microanalysis, 2015, 21, 1369-1370.	0.4	0
196	Investigation of the Structural and Electronic Properties of Pt/γ-Al2O3, a Model Catalyst System. Microscopy and Microanalysis, 2015, 21, 1655-1656.	0.4	0
197	Fast Imaging of Carbon Nanotube Carpet Growth by Environmental TEM. Microscopy and Microanalysis, 2015, 21, 2327-2328.	0.4	1
198	Low Angle Annular Dark Field Scanning Transmission Electron Microscopy is Sensitive to Oxidation State in CeO2 Nanoparticles. Microscopy and Microanalysis, 2015, 21, 239-240.	0.4	0

#	Article	IF	CITATIONS
199	The Role of Surface Passivation in Controlling Ge Nanowire Faceting. Nano Letters, 2015, 15, 8211-8216.	9.1	17
200	Complex structural dynamics of nanocatalysts revealed in Operando conditions by correlated imaging and spectroscopy probes. Nature Communications, 2015, 6, 7583.	12.8	118
201	Comparative in Operando Studies in Heterogeneous Catalysis: Atomic and Electronic Structural Features in the Hydrogenation of Ethylene over Supported Pd and Pt Catalysts. ACS Catalysis, 2015, 5, 1539-1551.	11.2	46
202	In situ visualization of metallurgical reactions in nanoscale Cu/Sn diffusion couples. Nanoscale, 2015, 7, 4984-4994.	5.6	27
203	Hierarchical Heterogeneity at the CeO <sub><i>x</i></sub> –TiO <sub>2</sub> Interface: Electronic and Geometric Structural Influence on the Photocatalytic Activity of Oxide on Oxide Nanostructures. Journal of Physical Chemistry C, 2015, 119, 2669-2679.	3.1	52
204	Corrigendum to "Enhancing the stability of copper chromite catalysts for the selective hydrogenation of furfural using ALD overcoating―[J. Catal. 317 (2014) 284–292]. Journal of Catalysis, 2015, 323, 165.	6.2	1
205	Ultrathin Europium Oxide Nanoplatelets: "Hidden―Parameters and Controlled Synthesis, Unusual Crystal Structure, and Photoluminescence Properties. Chemistry of Materials, 2015, 27, 965-974.	6.7	17
206	Strain and Stability of Ultrathin Ge Layers in Si/Ge/Si Axial Heterojunction Nanowires. Nano Letters, 2015, 15, 1654-1659.	9.1	24
207	Transitions from Near-Surface to Interior Redox upon Lithiation in Conversion Electrode Materials. Nano Letters, 2015, 15, 1437-1444.	9.1	97
208	Graphene-modified nanostructured vanadium pentoxide hybrids with extraordinary electrochemical performance for Li-ion batteries. Nature Communications, 2015, 6, 6127.	12.8	201
209	Mechanism and Enhanced Yield of Carbon Nanotube Growth on Stainless Steel by Oxygen-Induced Surface Reconstruction. Chemistry of Materials, 2015, 27, 932-937.	6.7	35
210	Synthesis of nanostructures in nanowires using sequential catalyst reactions. Nature Materials, 2015, 14, 820-825.	27.5	82
211	The role of interparticle heterogeneities in the selenization pathway of Cu–Zn–Sn–S nanoparticle thin films: a real-time study. Journal of Materials Chemistry C, 2015, 3, 7128-7134.	5.5	21
212	Characterization of V-shaped Defects in 4H-SiC Homoepitaxial Layers. Journal of Electronic Materials, 2015, 44, 1293-1299.	2.2	4
213	Effect of deposition pressure on the microstructure and thermoelectric properties of epitaxial ScN(001) thin films sputtered onto MgO(001) substrates. Journal of Materials Research, 2015, 30, 626-634.	2.6	34
214	Using Real-Time Electron Microscopy To Explore the Effects of Transition-Metal Composition on the Local Thermal Stability in Charged Li <sub><i>x</i></sub> Ni <sub><i>y</i></sub> Mn <sub><i>z</i></sub> Co <sub>1â€"<i>y</i>â€"<i>z</i></sub> Cathode Materials. Chemistry of Materials, 2015, 27, 3927-3935.	O<\$uD>2<	/sub>
215	Correlating Size and Composition-Dependent Effects with Magnetic, M¶ssbauer, and Pair Distribution Function Measurements in a Family of Catalytically Active Ferrite Nanoparticles. Chemistry of Materials, 2015, 27, 3572-3592.	6.7	77
216	Real-Time Observation of Morphological Transformations in II–VI Semiconducting Nanobelts via Environmental Transmission Electron Microscopy. Nano Letters, 2015, 15, 3303-3308.	9.1	13

#	Article	IF	CITATIONS
217	Solution-based synthesis and purification of zinc tin phosphide nanowires. Nanoscale, 2015, 7, 19317-19323.	5.6	5
218	Probing the active sites for water–gas shift over Pt/molybdenum carbide using multi-walled carbon nanotubes. Journal of Catalysis, 2015, 330, 442-451.	6.2	22
219	Striving Toward Noble-Metal-Free Photocatalytic Water Splitting: The Hydrogenated-Graphene–TiO <sub>2</sub> Prototype. Chemistry of Materials, 2015, 27, 6282-6296.	6.7	81
220	Sodiation Kinetics of Metal Oxide Conversion Electrodes: A Comparative Study with Lithiation. Nano Letters, 2015, 15, 5755-5763.	9.1	122
221	Superior performance of Ni–W–Ce mixed-metal oxide catalysts for ethanol steam reforming: Synergistic effects of W- and Ni-dopants. Journal of Catalysis, 2015, 321, 90-99.	6.2	47
222	9.0% efficient Cu <sub>2</sub> ZnSn(S,Se) <sub>4</sub> solar cells from selenized nanoparticle inks. Progress in Photovoltaics: Research and Applications, 2015, 23, 654-659.	8.1	205
223	Development of epitaxial Al <sub> <i>x</i> </sub> Sc <sub>1â^'<i>x</i> </sub> N for artificially structured metal/semiconductor superlattice metamaterials. Physica Status Solidi (B): Basic Research, 2015, 252, 251-259.	1.5	46
224	In Situ Visualization of Metallurgical Reactions in Nanoscale Cu/Sn Diffusion Couples. Microscopy and Microanalysis, 2015, 21, 943-944.	0.4	1
225	A method to determine fault vectors in 4H-SiC from stacking sequences observed on high resolution transmission electron microscopy images. Journal of Applied Physics, 2014, 116, 104905.	2.5	2
226	Comparative study of the alloying effect on the initial oxidation of Cu-Au(100) and Cu-Pt(100). Applied Physics Letters, 2014, 104, 121601.	3.3	15
227	Compositional Inhomogeneity of Multinary Semiconductor Nanoparticles: A Case Study of Cu <sub>2</sub> ZnSnS <sub>4</sub> . Chemistry of Materials, 2014, 26, 6955-6962.	6.7	26
228	Gas mixing system for imaging of nanomaterials under dynamic environments by environmental transmission electron microscopy. Review of Scientific Instruments, 2014, 85, 033704.	1.3	1
229	Critical review: Effects of complex interactions on structure and dynamics of supported metal catalysts. Journal of Vacuum Science and Technology A: Vacuum, Surfaces and Films, 2014, 32, .	2.1	31
230	Gas-phase epoxidation of propylene in the presence of H2 and O2 over small gold ensembles in uncalcined TS-1. Journal of Catalysis, 2014, 313, 104-112.	6.2	74
231	Cu2ZnSn(S,Se)4 solar cells from inks of heterogeneous Cu–Zn–Sn–S nanocrystals. Solar Energy Materials and Solar Cells, 2014, 123, 189-196.	6.2	34
232	A Manganese-Doped Barium Carbonate Cathode for Alkaline Batteries. Journal of the Electrochemical Society, 2014, 161, A835-A840.	2.9	19
233	Investigation of Changes in the Surface Structure of Li <sub><i>x</i></sub> Ni <sub>0.8</sub> Co <sub>0.15</sub> Al <sub>0.05</sub> O <sub>2</sub> Cathode Materials Induced by the Initial Charge. Chemistry of Materials, 2014, 26, 1084-1092.	6.7	308
234	Kesterite Cu <sub>2</sub> ZnSn(S,Se) <sub>4</sub> Absorbers Converted from Metastable, Wurtzite-Derived Cu <sub>2</sub> ZnSnS <sub>4</sub> Nanoparticles. Chemistry of Materials, 2014, 26, 3530-3534.	6.7	53

#	Article	IF	CITATIONS
235	Structural and catalytic differences in the effect of Co and Mo as promoters for Pt-based aqueous phase reforming catalysts. Applied Catalysis B: Environmental, 2014, 156-157, 236-248.	20.2	38
236	Epitaxial superlattices with titanium nitride as a plasmonic component for optical hyperbolic metamaterials. Proceedings of the National Academy of Sciences of the United States of America, 2014, 111, 7546-7551.	7.1	198
237	Effect of Co Loading on the Activity and Selectivity of PtCo Aqueous Phase Reforming Catalysts. ACS Catalysis, 2014, 4, 480-491.	11.2	38
238	Real time observation of ZnO nanostructure formation via the solid–vapor and solid–solid–vapor mechanisms. Nanoscale, 2014, 6, 6984.	5.6	4
239	TiN/(Al,Sc)N metal/dielectric superlattices and multilayers as hyperbolic metamaterials in the visible spectral range. Physical Review B, 2014, 90, .	3.2	52
240	Structure of catalyst particles from in-situ electron microscopy: a web themed issue. Chemical Communications, 2014, 50, 12417-12419.	4.1	5
241	An in situ transmission electron microscopy study of sintering and redispersion phenomena over size-selected metal nanoparticles: environmental effects. Physical Chemistry Chemical Physics, 2014, 16, 18176-18184.	2.8	31
242	Water-Gas Shift Reaction on Ni–W–Ce Catalysts: Catalytic Activity and Structural Characterization. Journal of Physical Chemistry C, 2014, 118, 2528-2538.	3.1	48
243	Synthesis of (CuInS2)0.5(ZnS)0.5 Alloy Nanocrystals and Their Use for the Fabrication of Solar Cells via Selenization. Chemistry of Materials, 2014, 26, 4060-4063.	6.7	17
244	Au Transport in Catalyst Coarsening and Si Nanowire Formation. Nano Letters, 2014, 14, 4554-4559.	9.1	13
245	Enhancing the stability of copper chromite catalysts for the selective hydrogenation of furfural using ALD overcoating. Journal of Catalysis, 2014, 317, 284-292.	6.2	65
246	Surface-Step-Induced Oscillatory Oxide Growth. Physical Review Letters, 2014, 113, 136104.	7.8	52
247	Investigating Local Degradation and Thermal Stability of Charged Nickel-Based Cathode Materials through Real-Time Electron Microscopy. ACS Applied Materials & Interfaces, 2014, 6, 15140-15147.	8.0	90
248	Correlating Atomic Structure and Transport in Suspended Graphene Nanoribbons. Nano Letters, 2014, 14, 4238-4244.	9.1	71
249	Determining the Resolution Limits of Electron-Beam Lithography: Direct Measurement of the Point-Spread Function. Nano Letters, 2014, 14, 4406-4412.	9.1	67
250	Surface Plasmon-Driven Water Reduction: Gold Nanoparticle Size Matters. Journal of the American Chemical Society, 2014, 136, 9842-9845.	13.7	301
251	Pore Structure and Bifunctional Catalyst Activity of Overlayers Applied by Atomic Layer Deposition on Copper Nanoparticles. ACS Catalysis, 2014, 4, 1554-1557.	11.2	58
252	Engineering the Activity and Lifetime of Heterogeneous Catalysts for Carbon Nanotube Growth via Substrate Ion Beam Bombardment. Nano Letters, 2014, 14, 4997-5003.	9.1	19

#	Article	IF	CITATIONS
253	Prolonged Hot Electron Dynamics in Plasmonicâ€Metal/Semiconductor Heterostructures with Implications for Solar Photocatalysis. Angewandte Chemie - International Edition, 2014, 53, 7887-7891.	13.8	349
254	Revealing the Atomic Restructuring of Pt–Co Nanoparticles. Nano Letters, 2014, 14, 3203-3207.	9.1	162
255	Rate-Dependent, Li-Ion Insertion/Deinsertion Behavior of LiFePO <sub>4</sub> Cathodes in Commercial 18650 LiFePO <sub>4</sub> Cells. ACS Applied Materials & Interfaces, 2014, 6, 3282-3289.	8.0	57
256	Adsorbate-Induced Structural Changes in 1–3 nm Platinum Nanoparticles. Journal of the American Chemical Society, 2014, 136, 9320-9326.	13.7	69
257	The Structural Evolution of V2O5 Nanocystals during Electrochemical Cycling Studied Using In operando Synchrotron Techniques. Electrochimica Acta, 2014, 136, 318-322.	5.2	17
258	Linking Performance with Particle Configuration on Bimetallic Pt/Co/MWCNT Catalysts for Aqueous Phase Reforming by Aberration Corrected STEM coupled with EELS. Microscopy and Microanalysis, 2014, 20, 182-183.	0.4	0
259	Fast Imaging of Carbon Nanotube Nucleation and Growth Processes using Environmental TEM. Microscopy and Microanalysis, 2014, 20, 1552-1553.	0.4	1
260	10.1063/1.4870085.1., 2014, , .		1
261	Noncrystalline-to-Crystalline Transformations in Pt Nanoparticles. Journal of the American Chemical Society, 2013, 135, 13062-13072.	13.7	71
262	In Situ Observation of the Effect of Nitrogen on Carbon Nanotube Synthesis. Chemistry of Materials, 2013, 25, 2921-2923.	6.7	26
263	Nature of the Mixed-Oxide Interface in Ceria–Titania Catalysts: Clusters, Chains, and Nanoparticles. Journal of Physical Chemistry C, 2013, 117, 14463-14471.	3.1	73
264	Microstructure of Bimetallic PtPd Catalysts under Oxidizing Conditions. ChemCatChem, 2013, 5, 2636-2645.	3.7	64
265	Revisiting the "In-clustering―question in InGaN through the use of aberration-corrected electron microscopy below the knock-on threshold. Applied Physics Letters, 2013, 102, .	3.3	43
266	Control of Metal Nanocrystal Size Reveals Metal-Support Interface Role for Ceria Catalysts. Science, 2013, 341, 771-773.	12.6	1,142
267	Correlating Structural Changes and Gas Evolution during the Thermal Decomposition of Charged Li <sub><i>x</i></sub> Ni <sub>0.8</sub> Co <sub>0.15</sub> Al <sub>0.05</sub> O <sub>2</sub> Cathode Materials. Chemistry of Materials, 2013, 25, 337-351.	6.7	317
268	Enhanced reaction rate for gas-phase epoxidation of propylene using H2 and O2 by Cs promotion of Au/TS-1. Journal of Catalysis, 2013, 308, 98-113.	6.2	92
269	High efficiency Cu <inf>2</inf> ZnSnS <inf>4</inf> nanocrystal ink solar cells through improved nanoparticle synthesis and selenization. , 2013, , .		2
270	Shape-Controlled Synthesis of Pt Nanocrystals: The Role of Metal Carbonyls. ACS Nano, 2013, 7, 645-653.	14.6	162

#	ARTICLE	IF	CITATIONS
271	A Titanium Nitride based Metamaterial for Applications in the Visible. , 2013, , .		0
272	Enhanced Pt/C catalyst stability using p-benzensulfonic acid functionalized carbon blacks as catalyst supports. Electrochimica Acta, 2013, 94, 172-181.	5.2	29
273	Resolution Limits of Electron-Beam Lithography toward the Atomic Scale. Nano Letters, 2013, 13, 1555-1558.	9.1	350
274	Steam Reforming of Ethanol on Ni/CeO <sub>2</sub> : Reaction Pathway and Interaction between Ni and the CeO <sub>2</sub> Support. ACS Catalysis, 2013, 3, 975-984.	11.2	210
275	Hydrogen-Induced Morphotropic Phase Transformation of Single-Crystalline Vanadium Dioxide Nanobeams. Nano Letters, 2013, 13, 1822-1828.	9.1	53
276	In Situ Liquid Cell Electron Microscopy of the Solution Growth of Au–Pd Core–Shell Nanostructures. Nano Letters, 2013, 13, 2964-2970.	9.1	164
277	Structural Modification of Graphene Sheets to Create a Dense Network of Defect Sites. Journal of Physical Chemistry Letters, 2013, 4, 1484-1488.	4.6	16
278	Engineering Catalytic Contacts and Thermal Stability: Gold/Iron Oxide Binary Nanocrystal Superlattices for CO Oxidation. Journal of the American Chemical Society, 2013, 135, 1499-1505.	13.7	122
279	Design of Pt–Pd Binary Superlattices Exploiting Shape Effects and Synergistic Effects for Oxygen Reduction Reactions. Journal of the American Chemical Society, 2013, 135, 42-45.	13.7	180
280	Heterogeneous Catalysts Need Not Be so "Heterogeneous― Monodisperse Pt Nanocrystals by Combining Shape-Controlled Synthesis and Purification by Colloidal Recrystallization. Journal of the American Chemical Society, 2013, 135, 2741-2747.	13.7	105
281	In situ atomic-scale visualization of oxide islanding during oxidation of Cu surfaces. Chemical Communications, 2013, 49, 10862.	4.1	54
282	Direct electron beam patterning of sub-5nm monolayer graphene interconnects. Proceedings of SPIE, 2013, , .	0.8	4
283	Cobalt Molybdenum Oxynitrides: Synthesis, Structural Characterization, and Catalytic Activity for the Oxygen Reduction Reaction. Angewandte Chemie - International Edition, 2013, 52, 10753-10757.	13.8	139
284	Preparation of High Surface Area Nano-Structured Graphene Composites. ECS Transactions, 2012, 41, 95-105.	0.5	8
285	Estimating the In-Plane Young's Modulus of Polycrystalline Films in MEMS. Journal of Microelectromechanical Systems, 2012, 21, 840-849.	2.5	19
286	Syntheses of Boron Nitride Nanotubes from Borazine and Decaborane Molecular Precursors by Catalytic Chemical Vapor Deposition with a Floating Nickel Catalyst. Chemistry of Materials, 2012, 24, 2872-2879.	6.7	46
287	Understanding the Chemistry of H <sub>2</sub> Production for 1-Propanol Reforming: Pathway and Support Modification Effects. ACS Catalysis, 2012, 2, 2316-2326.	11.2	29
288	Probing the gold active sites in Au/TS-1 for gas-phase epoxidation of propylene in the presence of hydrogen and oxygen. Journal of Catalysis, 2012, 296, 31-42.	6.2	88

#	Article	IF	CITATIONS
289	Heterogeneous nanoclusters assembled by PNA-templated double-stranded DNA. Nanoscale, 2012, 4, 6722.	5.6	12
290	Size and Support Effects for the Water–Gas Shift Catalysis over Gold Nanoparticles Supported on Model Al <sub>2</sub> O <sub>3</sub> and TiO <sub>2</sub> . Journal of the American Chemical Society, 2012, 134, 4700-4708.	13.7	380
291	Growth Pathways in Ultralow Temperature Ge Nucleation from Au. Nano Letters, 2012, 12, 5867-5872.	9.1	30
292	Counting Au catalytic sites for the water–gas shift reaction. Journal of Catalysis, 2012, 293, 94-102.	6.2	40
293	Revealing Correlation of Valence State with Nanoporous Structure in Cobalt Catalyst Nanoparticles by <i>In Situ</i> Environmental TEM. ACS Nano, 2012, 6, 4241-4247.	14.6	84
294	Step-Edge-Induced Oxide Growth During the Oxidation of Cu Surfaces. Physical Review Letters, 2012, 109, 235502.	7.8	103
295	Seeing atoms in three dimensions. Nature Materials, 2012, 11, 911-912.	27.5	11
296	Highly Active Pt <sub>3</sub> Pb and Core–Shell Pt <sub>3</sub> Pb–Pt Electrocatalysts for Formic Acid Oxidation. ACS Nano, 2012, 6, 2818-2825.	14.6	177
297	Controlling the Growth of Si/Ge Nanowires and Heterojunctions Using Silver–Gold Alloy Catalysts. ACS Nano, 2012, 6, 6407-6415.	14.6	77
298	Aqueous Phase Glycerol Reforming by PtMo Bimetallic Nano-Particle Catalyst: Product Selectivity and Structural Characterization. Topics in Catalysis, 2012, 55, 53-69.	2.8	62
299	Preparation of high-surface-area carbon nanoparticle/graphene composites. Carbon, 2012, 50, 3845-3853.	10.3	57
300	Reproducible preparation of Au/TS-1 with high reaction rate for gas phase epoxidation of propylene. Journal of Catalysis, 2012, 287, 178-189.	6.2	116
301	Utilizing the thermodynamic nanoparticle size effects for low temperature Pb-free solder. Materials Science and Engineering B: Solid-State Materials for Advanced Technology, 2012, 177, 197-204.	3.5	21
302	Silver layer instability in a SnO2/Ag/SnO2 trilayer on silicon. Thin Solid Films, 2012, 520, 6189-6195.	1.8	18
303	"Zero" drain-current drift of inversion-mode NMOSFET on InP (111)A surface. , 2011, , .		2
304	Differences in Catalytic Sites for CO Oxidation and Propylene Epoxidation on Au Nanoparticles. ACS Catalysis, 2011, 1, 1327-1330.	11.2	52
305	Built-in Electric Field Minimization in (In, Ga)N Nanoheterostructures. Nano Letters, 2011, 11, 4515-4519.	9.1	13
306	Controlled Growth of Ordered Nanopore Arrays in GaN. Nano Letters, 2011, 11, 535-540.	9.1	10

#	Article	IF	CITATIONS
307	Vacancies, twins, and the thermal stability of ultrafine-grained copper. Applied Physics Letters, 2011, 99, .	3.3	21
308	Control and characterization of individual grains and grain boundaries in graphene grown by chemical vapour deposition. Nature Materials, 2011, 10, 443-449.	27.5	1,356
309	Crystallization and electrochemical performance of La0.6Sr0.4Co0.2Fe0.8O3â^î^C-Ce0.8Gd0.2O1.9 thin film cathodes processed by single solution spray pyrolysis. Solid State Ionics, 2011, 203, 62-68.	2.7	6
310	Carbon-Based Supercapacitors Produced by Activation of Graphene. Science, 2011, 332, 1537-1541.	12.6	5,528
311	Truncated Ditetragonal Gold Prisms as Nanofacet Activators of Catalytic Platinum. Journal of the American Chemical Society, 2011, 133, 18074-18077.	13.7	66
312	Multimodal grain size distribution and high hardness in fine grained tungsten fabricated by spark plasma sintering. Materials Science & Engineering A: Structural Materials: Properties, Microstructure and Processing, 2011, 528, 5670-5677.	5.6	82
313	Enhancing the catalytic performance of Pt/C catalysts using steam-etched carbon blacks as a catalyst support. Carbon, 2011, 49, 256-265.	10.3	20
314	Fatigue performance improvement in AISI 4140 steel by dynamic strain aging and dynamic precipitation during warm laser shock peening. Acta Materialia, 2011, 59, 1014-1025.	7.9	230
315	Nanoscale graphite-supported Pt catalysts for oxygen reduction reactions in fuel cells. Electrochimica Acta, 2011, 56, 2566-2573.	5.2	33
316	Surface functionalized silica as a toolkit for studying aqueous phase palladium adsorption and mineralization on thiol moiety in the absence of external reducing agents. Journal of Colloid and Interface Science, 2011, 356, 31-36.	9.4	16
317	Desorption induced formation of negative nanowires in GaN. Journal of Crystal Growth, 2011, 324, 119-123.	1.5	4
318	Amorphous interface layer in thin graphite films grown on the carbon face of SiC. Applied Physics Letters, 2011, 99, 101904.	3.3	15
319	Kinetics of Congruent Vaporization of ZnO Islands. Physical Review Letters, 2011, 107, 146101.	7.8	10
320	Dislocation pinning effects induced by nano-precipitates during warm laser shock peening: Dislocation dynamic simulation and experiments. Journal of Applied Physics, 2011, 110, .	2.5	35
321	Laser direct write of silicon nanowires. Optical Engineering, 2011, 50, 104301.	1.0	7
322	Mechanism of vertical Ge nanowire nucleation on Si (111) during subeutectic annealing and growth. Journal of Materials Research, 2011, 26, 2744-2748.	2.6	5
323	Wear mechanisms and friction parameters for sliding wear of micron-scale polysilicon sidewalls. Sensors and Actuators A: Physical, 2010, 163, 373-382.	4.1	16
324	Empirical Study of Hall Bars on Few-Layer Graphene on C-Face 4H-SiC. Journal of Electronic Materials, 2010, 39, 2696-2701.	2.2	11

#	Article	IF	CITATIONS
325	Investigation of carbon corrosion in polymer electrolyte fuel cells using steam etching. Materials Chemistry and Physics, 2010, 123, 761-766.	4.0	36
326	Mechanism of dynamic structural reorganization in polyoxometalate catalysts. Journal of Catalysis, 2010, 270, 40-47.	6.2	18
327	The effects of cubic stiffness on fatigue characterization resonator performance. Sensors and Actuators A: Physical, 2010, 157, 228-234.	4.1	10
328	Quantitative study of Au(III) and Pd(II) ion biosorption on genetically engineered Tobacco mosaic virus. Journal of Colloid and Interface Science, 2010, 342, 455-461.	9.4	51
329	Preparation and Characterization of Graphitic Particles as Alternative Support for Oxygen Reduction Reaction Catalysts in Fuel Cells. ECS Transactions, 2010, 33, 533-544.	0.5	0
330	Enhancing the Catalytic Performance of Pt/C Catalysts Using Steam-Etched Carbon Blacks as a Catalyst Support. ECS Transactions, 2010, 33, 507-531.	0.5	2
331	(Invited) Fabrication and Properties of Abrupt Si-Ge Heterojunction Nanowire Structures. ECS Transactions, 2010, 33, 671-680.	0.5	1
332	Evolution, Activity, and Lifetime of Alumina-supported Fe Catalyst During Super Growth of Single-walled Carbon Nanotube Carpets: Influence of the Type of Alumina. Materials Research Society Symposia Proceedings, 2010, 1258, 1.	0.1	1
333	Large-scale graphitic thin films synthesized on Ni and transferred to insulators: Structural and electronic properties. Journal of Applied Physics, 2010, 107, .	2.5	83
334	GaN nanostructure design for optimal dislocation filtering. Journal of Applied Physics, 2010, 108, 074313.	2.5	10
335	Nucleation of highly dense nanoscale precipitates based on warm laser shock peening. Journal of Applied Physics, 2010, 108, .	2.5	47
336	Step-Flow Kinetics in Nanowire Growth. Physical Review Letters, 2010, 105, 195502.	7.8	79
337	Fabrication of conductive interconnects by Ag migration in Cu–Ag core-shell nanoparticles. Applied Physics Letters, 2010, 96, .	3.3	68
338	Formation of Au/Pd Alloy Nanoparticles on TMV. Journal of Nanomaterials, 2010, 2010, 1-6.	2.7	29
339	Nanomanipulation of ridges in few-layer epitaxial graphene grown on the carbon face of 4H-SiC. New Journal of Physics, 2010, 12, 125009.	2.9	17
340	Structure, Growth Kinetics, and Ledge Flow during Vaporâ^'Solidâ^'Solid Growth of Copper-Catalyzed Silicon Nanowires. Nano Letters, 2010, 10, 514-519.	9.1	136
341	Cross-sectional transmission electron microscopy of thin graphite films grown by chemical vapor deposition. Diamond and Related Materials, 2010, 19, 143-146.	3.9	5
342	Dislocation Filtering in GaN Nanostructures. Nano Letters, 2010, 10, 1568-1573.	9.1	110

#	Article	IF	CITATIONS
343	Influence of Alumina Type on the Evolution and Activity of Alumina-Supported Fe Catalysts in Single-Walled Carbon Nanotube Carpet Growth. ACS Nano, 2010, 4, 895-904.	14.6	201
344	Biotemplated Aqueous-Phase Palladium Crystallization in the Absence of External Reducing Agents. Nano Letters, 2010, 10, 3863-3867.	9.1	70
345	III-nitride nanopyramid light emitting diodes grown by organometallic vapor phase epitaxy. Journal of Applied Physics, 2010, 108, 044303.	2.5	26
346	Genesis and Evolution of Surface Species during Pt Atomic Layer Deposition on Oxide Supports Characterized by in Situ XAFS Analysis and Waterâ^'Gas Shift Reaction. Journal of Physical Chemistry C, 2010, 114, 9758-9771.	3.1	124
347	Metallic Corner Atoms in Gold Clusters Supported on Rutile Are the Dominant Active Site during Waterâ^'Gas Shift Catalysis. Journal of the American Chemical Society, 2010, 132, 14018-14020.	13.7	170
348	Biomagnetic Glasses: Preparation, Characterization, and Biosensor Applications. Langmuir, 2010, 26, 4320-4326.	3.5	46
349	Fabrication of 7.2% Efficient CZTSSe Solar Cells Using CZTS Nanocrystals. Journal of the American Chemical Society, 2010, 132, 17384-17386.	13.7	903
350	Evolution in Catalyst Morphology Leads to Carbon Nanotube Growth Termination. Journal of Physical Chemistry Letters, 2010, 1, 918-922.	4.6	177
351	Catalyst and catalyst support morphology evolution in single-walled carbon nanotube supergrowth: Growth deceleration and termination. Journal of Materials Research, 2010, 25, 1875-1885.	2.6	43
352	Transmission Electron Microscopy Observation of Corrosion Behaviors of Platinized Carbon Blacks under Thermal and Electrochemical Conditions. Journal of the Electrochemical Society, 2010, 157, B906.	2.9	91
353	Investigation of the Carbon Corrosion Process for Polymer Electrolyte Fuel Cells Using a Rotating Disk Electrode Technique. Journal of the Electrochemical Society, 2010, 157, B1138.	2.9	33
354	Investigation of the Carbon Corrosion Process for Polymer Electrolyte Fuel Cells Using a Rotating Disk Electrode Technique. ECS Transactions, 2010, 33, 1281-1294.	0.5	6
355	Comment on "Size-Dependent Melting Properties of Small Tin Particles: Nanocalorimetric Measurements― Physical Review Letters, 2010, 104, 189601.	7.8	9
356	Formation of the ST12 phase in nanocrystalline Ge at ambient pressure. Journal of Materials Chemistry, 2010, 20, 331-337.	6.7	23
357	Determination of Size Effects during the Phase Transition of a Nanoscale Au-Si Eutectic. Physical Review Letters, 2009, 103, 155701.	7.8	53
358	Early Stage Strong Metal Support Interaction (SMSI) Effects in an Experimental Titania-Supported Platinum Catalyst An Environmental TEM Study. Microscopy and Microanalysis, 2009, 15, 1066-1067.	0.4	7
359	Formation of Compositionally Abrupt Axial Heterojunctions in Silicon-Germanium Nanowires. Science, 2009, 326, 1247-1250.	12.6	303
360	Fabrication of ZnS nanoparticle chains on a protein template. Journal of Nanoparticle Research, 2009, 11, 2031-2041.	1.9	14

#	Article	IF	CITATIONS
361	The Use of Polyethyleneimine to Control the Growthâ€Front Morphology of Electrochemically Deposited Gold Nanowires for Engineered Nanogap Electrodes. Small, 2009, 5, 2387-2391.	10.0	3
362	Pseudomorphic stabilization of rocksalt GaN in TiN/GaN multilayers and superlattices. Physical Review B, 2009, 80, .	3.2	15
363	Rapid and Scalable Reduction of Dense Surface-Supported Metal-Oxide Catalyst with Hydrazine Vapor. ACS Nano, 2009, 3, 1897-1905.	14.6	27
364	Preferential Growth of Single-Walled Carbon Nanotubes with Metallic Conductivity. Science, 2009, 326, 116-120.	12.6	397
365	Role of Water in Super Growth of Single-Walled Carbon Nanotube Carpets. Nano Letters, 2009, 9, 44-49.	9.1	371
366	0.8-V Supply Voltage Deep-Submicrometer Inversion-Mode \$hbox{In}_{0.75}hbox{Ga}_{0.25}hbox{As}\$ MOSFET. IEEE Electron Device Letters, 2009, 30, 700-702.	3.9	91
367	Understanding Growth Termination of Single-Walled Carbon Nanotube Carpets by Documenting the Evolution of Catalyst Morphology with the Transmission Electron Microscope. Microscopy and Microanalysis, 2009, 15, 1176-1177.	0.4	5
368	Effect of Catalyst Composition on Si Nanowire Growth Kinetics. Microscopy and Microanalysis, 2009, 15, 1226-1227.	0.4	0
369	Real-time observations with electron microscopy. Materials Today, 2008, 11, 50-58.	14.2	44
370	Effect of post-release sidewall morphology on the fracture and fatigue properties of polycrystalline silicon structural films. Sensors and Actuators A: Physical, 2008, 147, 553-560.	4.1	28
371	Electrical properties of ZnO nanowire field effect transistors by surface passivation. Colloids and Surfaces A: Physicochemical and Engineering Aspects, 2008, 313-314, 378-382.	4.7	47
372	Development of CuInSe <sub>2</sub> Nanocrystal and Nanoring Inks for Low-Cost Solar Cells. Nano Letters, 2008, 8, 2982-2987.	9.1	545
373	Nanotubes reveal their true strength. Nature Nanotechnology, 2008, 3, 586-587.	31.5	6
374	Organometallic vapor phase epitaxial growth of GaN on ZrNâ^•AlNâ^•Si substrates. Applied Physics Letters, 2008, 93, 023109.	3.3	17
375	Role of Molecular Surface Passivation in Electrical Transport Properties of InAs Nanowires. Nano Letters, 2008, 8, 49-55.	9.1	107
376	Detection of Single Atoms and Buried Defects in Three Dimensions by Aberration-Corrected Electron Microscope with 0.5-A Information Limit. Microscopy and Microanalysis, 2008, 14, 469-477.	0.4	266
377	Micron-Scale Friction and Sliding Wear of Polycrystalline Silicon Thin Structural Films in Ambient Air. Journal of Microelectromechanical Systems, 2008, 17, 1144-1154.	2.5	46
378	Double-Walled Boron Nitride Nanotubes Grown by Floating Catalyst Chemical Vapor Deposition. Nano Letters, 2008, 8, 3298-3302.	9.1	109

#	Article	IF	CITATIONS
379	Kinetics of Individual Nucleation Events Observed in Nanoscale Vapor-Liquid-Solid Growth. Science, 2008, 322, 1070-1073.	12.6	207
380	Peeling Force Spectroscopy:  Exposing the Adhesive Nanomechanics of One-Dimensional Nanostructures. Nano Letters, 2008, 8, 544-550.	9.1	75
381	Visualizing the Behavior of Dislocations—Seeing is Believing. MRS Bulletin, 2008, 33, 122-131.	3.5	33
382	Nanometer-scale sharpness in corner-overgrown heterostructures. Applied Physics Letters, 2008, 93, 193117.	3.3	10
383	<i>In Situ</i> Transmission Electron Microscopy. MRS Bulletin, 2008, 33, 83-90.	3.5	44
384	Protein-templated semiconductor nanoparticle chains. Nanotechnology, 2008, 19, 275602.	2.6	24
385	Molecular beam epitaxy growth of InAs and In[sub 0.8]Ga[sub 0.2]As channel materials on GaAs substrate for metal oxide semiconductor field effect transistor applications. Journal of Vacuum Science & Technology B, 2008, 26, 1187.	1.3	0
386	Directed self-assembly of quantum structures by nanomechanical stamping using probe tips. Nanotechnology, 2008, 19, 015301.	2.6	36
387	Inter- and Intra-Agglomerate Fracture in Nanocrystalline Nickel. Physical Review Letters, 2008, 100, 105502.	7.8	31
388	Nanoscale mechanisms of misfit dislocation propagation in undulated Si1â^'xGex/Si(100) epitaxial thin films. Nanotechnology, 2007, 18, 165705.	2.6	4
389	Chapter 78 In situ Nanoindentation in a Transmission Electron Microscope. Dislocations in Solids, 2007, , 453-497.	1.6	2
390	Realization of highly reproducible ZnO nanowire field effect transistors with n-channel depletion and enhancement modes. Applied Physics Letters, 2007, 90, 243103.	3.3	52
391	An electron microscopy study of wear in polysilicon microelectromechanical systems in ambient air. Thin Solid Films, 2007, 515, 3259-3266.	1.8	37
392	In situ nanoindentation in the TEM. Materials Today, 2007, 10, 59-60.	14.2	53
393	Vertical single- and double-walled carbon nanotubes grown from modified porous anodic alumina templates. Nanotechnology, 2006, 17, 3925-3929.	2.6	59
394	A new view of the onset of plasticity during the nanoindentation of aluminium. Nature Materials, 2006, 5, 697-702.	27.5	398
395	Graphene-based composite materials. Nature, 2006, 442, 282-286.	27.8	11,655
396	In situ TEM nanoindentation and dislocation-grain boundary interactions: a tribute to David Brandon. Journal of Materials Science, 2006, 41, 7704-7719.	3.7	101

#	Article	IF	CITATIONS
397	Mechanically Biased Self-Assembly of Quantum Dots by Nanoindentation. Materials Research Society Symposia Proceedings, 2006, 921, 1.	0.1	0
398	Fabrication and characterization of solid-state nanopores using a field emission scanning electron microscope. Applied Physics Letters, 2006, 88, 103109.	3.3	73
399	Nanoscale dislocation patterning by ultralow load indentation. Applied Physics Letters, 2005, 87, 073108.	3.3	26
400	Atomic and Electronic Structure of Mixed and Partial Dislocations in GaN. Physical Review Letters, 2005, 94, 025504.	7.8	59
401	Analysis of Nanoscale Deformation in GaAs(100): Towards Patterned Growth of Quantum Dots. Materials Research Society Symposia Proceedings, 2005, 864, 571.	0.1	0
402	Investigation of femtosecond laser assisted nano and microscale modifications in lithium niobate. Journal of Applied Physics, 2005, 97, 074316.	2.5	56
403	Faceted and Vertically Aligned GaN Nanorod Arrays Fabricated without Catalysts or Lithography. Nano Letters, 2005, 5, 1847-1851.	9.1	98
404	Metal delocalization and surface decoration in direct-write nanolithography by electron beam induced deposition. Applied Physics Letters, 2004, 85, 49-51.	3.3	39
405	In-Situ Electron Microscopy Studies of the Effect of Solute Segregation on Grain Boundary Anisotropy and Mobility in an Al-Zr Alloy. Materials Research Society Symposia Proceedings, 2004, 839, 171.	0.1	1
406	Dislocation–grain boundary interactions in martensitic steel observed through in situ nanoindentation in a transmission electron microscope. Journal of Materials Research, 2004, 19, 3626-3632.	2.6	127
407	Direct observations of incipient plasticity during nanoindentation of Al. Journal of Materials Research, 2004, 19, 176-182.	2.6	99
408	Using the FIB to characterize nanoparticle materials. Journal of Microscopy, 2004, 214, 222-236.	1.8	16
409	Characteristic dimensions and the micro-mechanisms of fracture and fatigue in `nano' and `bio' materials. International Journal of Fracture, 2004, 128, 1-15.	2.2	40
410	Investigation of Femtosecond Laser-assisted Micromachining of Lithium Niobate. CIRP Annals - Manufacturing Technology, 2004, 53, 187-190.	3.6	19
411	Structural damage in boron carbide under contact loading. Acta Materialia, 2004, 52, 3921-3927.	7.9	132
412	Direct observation of deformation-induced grain growth during the nanoindentation of ultrafine-grained Al at room temperature. Acta Materialia, 2004, 52, 5381-5387.	7.9	346
413	Effects of solute Mg on grain boundary and dislocation dynamics during nanoindentation of Al–Mg thin films. Acta Materialia, 2004, 52, 5783-5790.	7.9	141
414	Rapid Prototyping of Site-Specific Nanocontacts by Electron and Ion Beam Assisted Direct-Write Nanolithography. Nano Letters, 2004, 4, 2059-2063.	9.1	115

#	Article	IF	CITATIONS
415	Grain Boundary-Mediated Plasticity in Nanocrystalline Nickel. Science, 2004, 305, 654-657.	12.6	803
416	In-situ nanoindentation of epitaxial TiN/MgO (001) in a transmission electron microscope. Journal of Electronic Materials, 2003, 32, 1023-1027.	2.2	29
417	Surface characterization of metal nanoparticles. Materials Science & Engineering A: Structural Materials: Properties, Microstructure and Processing, 2003, 359, 261-268.	5.6	79
418	An off-normal fibre-like texture in thin films on single-crystal substrates. Nature, 2003, 426, 641-645.	27.8	181
419	Watching GaN Nanowires Grow. Nano Letters, 2003, 3, 867-869.	9.1	188
420	Nanoscale surface and subsurface defects induced in lithium niobate by a femtosecond laser. Applied Physics Letters, 2003, 83, 4420-4422.	3.3	28
421	Origin of the orientation ratio in sputtered longitudinal media. Journal of Applied Physics, 2003, 93, 7393-7395.	2.5	2
422	Nitride-mediated epitaxy of CoSi2 on Si(001). Applied Physics Letters, 2003, 82, 1833-1835.	3.3	33
423	Nitrogen Effects on Crystallization Kinetics of Amorphous TiO <sub><i>x</i></sub> N <sub><i>y</i></sub> Thin Films. Journal of Materials Research, 2002, 17, 550-555.	2.6	34
424	Dynamical x-ray microscopy investigation of electromigration in passivated inlaid Cu interconnect structures. Applied Physics Letters, 2002, 81, 2535-2537.	3.3	44
425	Mechanism of fatigue in micron-scale films of polycrystalline silicon for microelectromechanical systems. Applied Physics Letters, 2002, 80, 1532-1534.	3.3	96
426	In-situ transmission electron microscopy study of the nanoindentation behavior of Al. Journal of Electronic Materials, 2002, 31, 958-964.	2.2	47
427	A reaction-layer mechanism for the delayed failure of micron-scale polycrystalline silicon structural films subjected to high-cycle fatigue loading. Acta Materialia, 2002, 50, 3579-3595.	7.9	189
428	Quantitativein situnanoindentation in an electron microscope. Applied Physics Letters, 2001, 79, 1625-1627.	3.3	157
429	Development of a Nanoindenter for In Situ Transmission Electron Microscopy. Microscopy and Microanalysis, 2001, 7, 507-517.	0.4	97
430	Phenomenological description of grain growth stagnation for nanocrystalline films and powders. Journal of Materials Research, 2001, 16, 1090-1095.	2.6	5
431	Enhancement of dislocation velocities by stress-assisted kink nucleation at the native oxide/SiGe interface. Applied Physics Letters, 2001, 79, 335-337.	3.3	7
432	Microstructural properties of (Ba, Sr)TiO3 films fabricated from BaF2/SrF2/TiO2 amorphous multilayers using the combinatorial precursor method. Journal of Applied Physics, 2001, 90, 2474-2478.	2.5	17

#	Article	IF	CITATIONS
433	Development of a Nanoindenter for In Situ Transmission Electron Microscopy. Microscopy and Microanalysis, 2001, 7, 507-517.	0.4	45
434	Structural Characterization Of Laser Lift-Off GaN. Materials Research Society Symposia Proceedings, 2000, 617, 351.	0.1	4
435	Real Time Observations of Dislocation-Mediated Plasticity in the Epitaxial AI (011)/Si(100) Thin Film System. Materials Research Society Symposia Proceedings, 2000, 619, 27.	0.1	5
436	Real Time Observation and Characterization of Dislocation Motion, Nitrogen Desorption and Nanopipe Formation in GaN. Materials Research Society Symposia Proceedings, 2000, 622, 581.	0.1	3
437	In-situ TEM observations of abnormal grain growth, coarsening, and substrate de-wetting in nanocrystalline Ag thin films. Thin Solid Films, 2000, 370, 54-62.	1.8	85
438	TEM annealing study of normal grain growth in silver thin films. Thin Solid Films, 2000, 379, 133-138.	1.8	81
439	<i>In-situ</i> transmission electron microscopy studies of the interaction between dislocations in strained SiGe/Si (001) heterostructures. Philosophical Magazine A: Physics of Condensed Matter, Structure, Defects and Mechanical Properties, 2000, 80, 2159-2200.	0.6	31
440	Analysis of twin defects in GaAs(111)B molecular beam epitaxy growth. Journal of Vacuum Science & Technology an Official Journal of the American Vacuum Society B, Microelectronics Processing and Phenomena, 2000, 18, 1566.	1.6	31
441	New Mechanism for Dislocation Blocking in Strained Layer Epitaxial Growth. Physical Review Letters, 2000, 84, 947-950.	7.8	42
442	Structural and chemical characterization of free-standing GaN films separated from sapphire substrates by laser lift-off. Applied Physics Letters, 2000, 77, 1819.	3.3	53
443	Analysis of electron intensity as a function of aperture size in energy-filtered transmission electron microscope imaging. Ultramicroscopy, 1999, 80, 221-236.	1.9	16
444	Strain Accommodation and Relief in <font>GeSi</font> / <font>Si</font> Heteroepitaxy. Series on Directions in Condensed Matter Physics, 1999, , 299-367.	0.1	8
445	Effect of the surface upon misfit dislocation velocities during the growth and annealing of SiGe/Si (001) heterostructures. Journal of Applied Physics, 1998, 83, 1931-1937.	2.5	43
446	In Situ Studies of the Interaction of Dislocations with Point Defects during Annealing of Ion Implanted Si/SiGe/Si (001) Heterostructures. Microscopy and Microanalysis, 1998, 4, 294-307.	0.4	39
447	Suppression of boron transient enhanced diffusion in SiGe heterojunction bipolar transistors by carbon incorporation. Applied Physics Letters, 1997, 70, 3125-3127.	3.3	51
448	Equilibrium and metastable strained layer semiconductor heterostructures. Current Opinion in Solid State and Materials Science, 1996, 1, 21-28.	11.5	6
449	Stacking Fault Formation via 2D Nucleation in PVT Grown 4H-SiC. Materials Science Forum, 0, 821-823, 85-89.	0.3	2